

Journal Pre-proof

A self-assembled, ROS-responsive Janus-prodrug for targeted therapy of inflammatory bowel disease

Shanshan Li, Aiqing Xie, Hui Li, Xiang Zou, Qixiong Zhang



PII: S0168-3659(19)30618-2
DOI: <https://doi.org/10.1016/j.jconrel.2019.10.054>
Reference: COREL 10003

To appear in:

Received Date: 30 August 2019
Revised Date: 23 October 2019
Accepted Date: 30 October 2019

Please cite this article as: Li S, Xie A, Li H, Zou X, Zhang Q, A self-assembled, ROS-responsive Janus-prodrug for targeted therapy of inflammatory bowel disease, *Journal of Controlled Release* (2019), doi: <https://doi.org/10.1016/j.jconrel.2019.10.054>

This is a PDF file of an article that has undergone enhancements after acceptance, such as the addition of a cover page and metadata, and formatting for readability, but it is not yet the definitive version of record. This version will undergo additional copyediting, typesetting and review before it is published in its final form, but we are providing this version to give early visibility of the article. Please note that, during the production process, errors may be discovered which could affect the content, and all legal disclaimers that apply to the journal pertain.

© 2019 Published by Elsevier.

A self-assembled, ROS-responsive Janus-prodrug for targeted therapy of inflammatory bowel disease

Shanshan Li ¹, Aiqing Xie ¹, Hui Li ², Xiang Zou ^{1,*}, Qixiong Zhang ^{3,*}

1. College of Pharmaceutical Sciences, Southwest University, Chongqing 400715, China

2. College of Chemical Engineering, Sichuan University, Chengdu 610065, China.

3. College of Pharmacy, Third Military Medical University, Chongqing 400038, China

Corresponding authors:

Dr. Qixiong Zhang

Department of Pharmaceutics

Third Military Medical University

30 Gaotanyan Main St., Chongqing 400038, China

E-mail: qixiongzhang@outlook.com

Prof. Xiang Zou

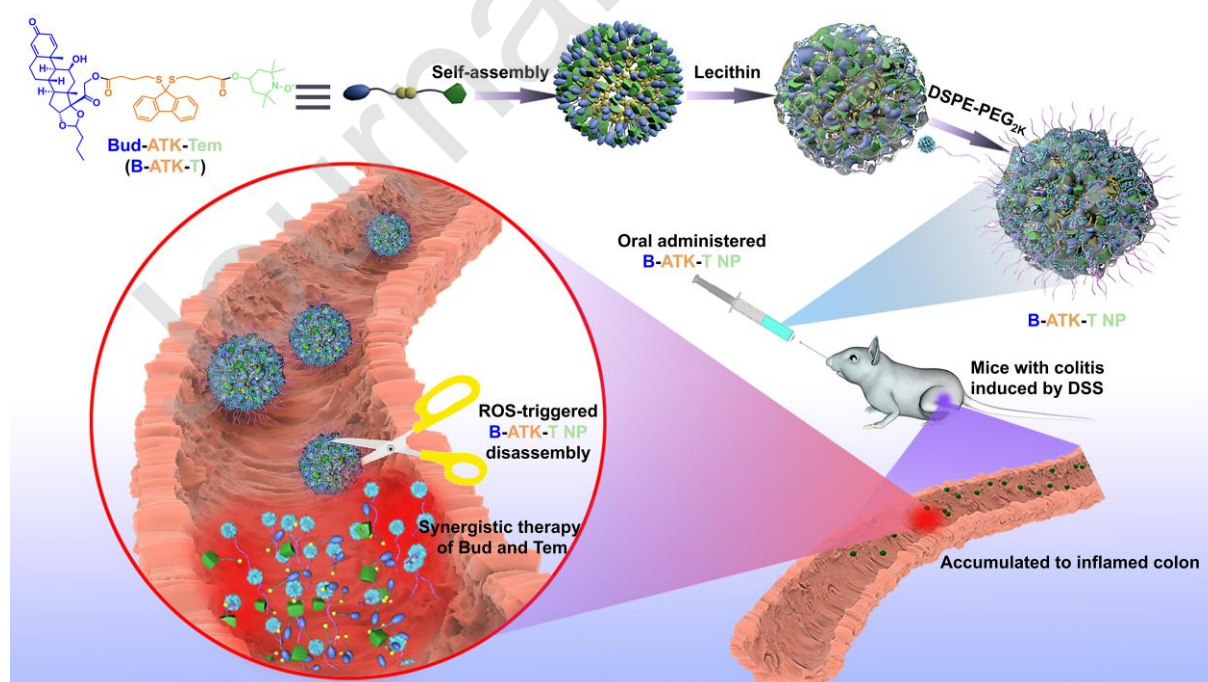
College of Pharmaceutical Sciences

Southwest University

2 Tiansheng Road, Chongqing 400715, China

E-mail: zhx1030@swu.edu.cn

Graphical abstract



Highlights

- Budesonide and tempol were linked by aromatized thioketal to form Janus-prodrug.
- Self-assembled prodrug B-ATK-T NP exhibited extremely high drug loading capacity.
- A broad ROS triggered the simultaneous release of two drugs from B-ATK-T NP.
- B-ATK-T NP could accumulate in inflamed colon and relieve colitis by oral route.

Abstract

A self-assembled and oxidation-degradable Janus-prodrug, termed as Bud-ATK-Tem (B-ATK-T), was fabricated by ROS-responsive aromatized thioketal (ATK) linked anti-inflammatory drug budesonide (Bud) and antioxidant tempol (Tem). Benefiting from the hydrophobic interactions and π - π stacking interactions of ATK, prodrug B-ATK-T could self-assemble into nanoparticles (NP) in water containing lecithin and DSPE-PEG_{2K}. The morphology of B-ATK-T NP (approximate 100-120 nm) was confirmed to be regular spherical by transmission electron microscope. B-ATK-T NP was endowed high drug loading content with 41.23% for Bud and 15.55% for Tem. The rapid drug release from B-ATK-T NP proceeded in an extensive reactive oxygen species (ROS)-dependent manner. More than 98% of Bud and Tem in B-ATK-T NP could release in the mimic inflammation microenvironment or phorbol-12-myristate-13-acetate (PMA)-stimulated macrophages within short time. The release of drugs in a simultaneous and proportional manner ensures that B-ATK-T NP can increase the combined efficacy of anti-inflammation and anti-oxidation. It is worth noting that B-ATK-T NP could be passively accumulated and dramatically increasing the maximum drugs concentration in the inflamed colon of mice with inflammatory bowel disease (IBD) by oral route, and avoiding potential systemic side effects. B-ATK-T NP could not only relieve colitis via inhibiting the expression of oxidative and proinflammatory mediators more than combination of free drugs, but also significantly reduce colitis-caused death. Taken together, the self-assembled, Janus-prodrug B-ATK-T NP is a promising candidate therapies for IBD, even for other inflammatory diseases.

Keywords: self-assembled; ROS-responsive; Janus-prodrug; site-specific therapy; inflammatory bowel disease

1. Introduction

Inflammatory bowel disease (IBD) is a typical inflammatory colorectal disease that adversely affects millions of patients around the world [1-4]. Administration of anti-inflammatory drugs is one of the preferred therapies for IBD [5, 6]. Budesonide (Bud), a new type of glucocorticoid anti-inflammatory drug, has been recommended by American Gastrointestinal Society as the “first-choice” drug for the treatment of mild-to-moderate ulcerative colitis [7, 8]. However, due to the first-pass effect, low oral bioavailability, large volume of distribution and high liver clearance of Bud, the local drug concentration in colon is too low to achieve desired efficacy [9]. Although the Bud rectal foam formation (Uceris[®], Salix Pharmaceuticals Inc.) has been clinically used, the rectal administration is inconvenience for patients [10, 11]. Meanwhile, IBD is also considered to be closely related to oxidative stress [12], and the local excess reactive oxygen species (ROS) promotes the development of IBD [13-15]. Some of the studies proved that antioxidant tempol (Tem) could alleviate DSS-induced

colitis by scavenging ROS [16-18]. Nevertheless, the strong hydrophilicity and short half-life of Tem make it difficult to be directly delivered to colon by oral administration. In view of the important roles of oxidative stress and inflammatory immune response in IBD, the combination of Bud and Tem therapy may provide a new effective strategy for the treatment of colitis.

Drug combination therapy has been used as an effective treatment for certain types of diseases for decades [19-21]. But in many cases, the multiple physicochemical properties, pharmacokinetics, and pharmacodynamics of a combination pharmaceutical formulation prevent components from reaching abnormal tissues/cells in desired proportions and duration, resulting in undesirable antagonism and increased non-specific toxicity [22]. Although several varieties of nanoscale delivery tools including liposome [23], polymer-drug conjugates [24], polymeric micelles [25], and protein-based nanoparticles [26] were determined to effectively deliver combination drugs to lesions, only few of them have undergone clinical trials [27-29]. Because most of the nanocarrier systems have low drug loading capacity and toxicity to kidneys or other organs during degradation, metabolism and excretion of nanocarriers [30-32].

Under such circumstances, drug-drug conjugates systems have been proposed as a new strategy because of the high drug loading capacity and low side effects [33, 34]. Several studies have established drug self-delivery systems, such as nanoparticles of irinotecan-chlorambucil [35], irinotecan-bendamustine [36], floxuridine-bendamustine [37], methotrexate-gemcitabine [38] and indomethacin-paclitaxel [39]. It is well known that an ideal drug self-delivery system should be able to achieve targeted and effective drug release [40]. However, current studies mainly focused on construction of drug self-delivery nanosystems by using amphiphilic features based on hydrophobic-hydrophilic drug conjugates with non-responsive covalent bonds (ester bond, etc.), resulting in unsuccessful on-demand release of drugs.

Herein, based on the aberrantly increased ROS at inflamed sites in IBD, a ROS-sensitive aromatized thioketal (ATK) linker was introduced to fabricate an oxidation-degradable, self-assembled Janus-prodrug Bud-ATK-Tem (B-ATK-T). Since widely reported acetone-based thioketal (TK) does not have sufficient hydrophobicity for self-assembly into nano-system, inspired by the π -conjugated TK molecule developed by M. Ueda et al. [41], ATK linker with both hydrophobicity and π - π stacking interactions were contributed to self-assemble Janus-prodrug B-ATK-T nanoparticles (B-ATK-T NP). As depicted in **Figure 1**, orally administered B-ATK-T NP could be passively targeted to the inflamed colon induced by dextran sodium sulfate (DSS) and simultaneously released Bud and Tem under the trigger of ROS in colitic tissues. B-ATK-T NP was supposed to enhance the drug concentration in colon and improved the effect of drug combination to alleviate colitis by more convenient oral route.

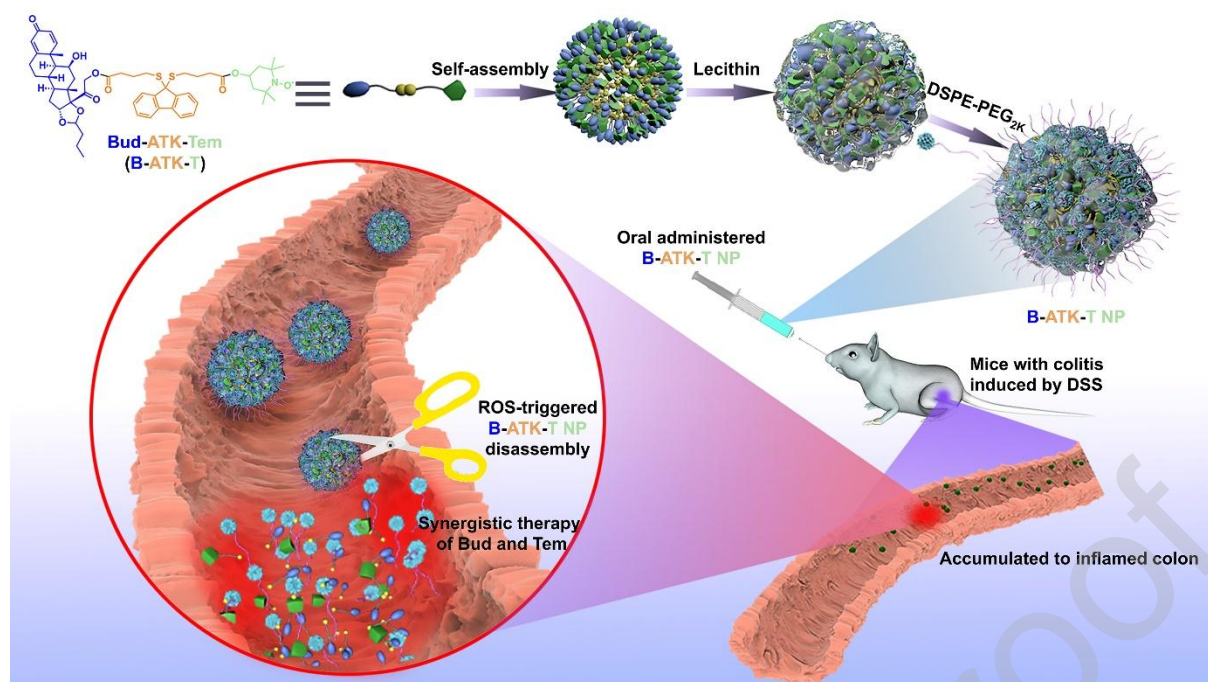


Figure 1. Schematic representation of the aromatized thioketal-bridged Janus-prodrug nanoassemblies and the ROS-responsive drug release in inflammation sites. The nanoassemblies were constructed by B-ATK-T Janus-prodrug. The DSPE-PEG_{2k} was utilized to prepare PEGylated surface. After B-ATK-T NP was delivered to inflammatory sites, on-demand drug release could be achieved through the ROS-responsive capability of thioketal bonds in the presence of overproduced ROS.

2. Materials and methods

2.1. Materials

4-Bromobutanoic acid and thiourea were purchased from TCI (Tokyo, Japan). 9-Fluorenone, trifluoroacetic acid (TFA), anhydrous N, N-dimethylformamide (DMF) and anhydrous dichloromethane (DCM) were supplied by J&K Scientific Ltd. (China). Dicyclohexylcarbodiimide (DCC), 4-dimethylaminopyridine (DMAP), pepsin, trypsin, 4-Hydroxy-TEMPO (Tem) and phorbol-12-myristate-13-acetate (PMA) were obtained from Sigma-Aldrich (USA). Budesonide (Bud) was purchased from MedChemExpress (USA). 1, 2-Distearoyl-sn-glycero-3-phosphoethanolamine-N-[(carbonyl-methoxy poly-(ethylene glycol)-2000) (DSPE-PEG_{2k}) and poly (lactide-co-glycolide) (PLGA, 75:25, with intrinsic viscosity of 0.50-0.65) were obtained from Xi'an Ruixi Biological Technology Co., Ltd (China). Dulbecco's Modified Eagle's medium (DMEM), fetal bovine serum (FBS), and trypsin for cell culture were purchased from Gibco (USA). 1, 1'-Dioctadecyl-3, 3, 3', 3'-tetramethylindocarbocyanine perchlorate (DiI) was obtained from MedChemExpress (USA). FITC Annexin V Apoptosis Detection Kits with 7-AAD was purchased from Biogend (USA), while dextran sulfate sodium (DSS, $M_w = 36-50$ kDa) was purchased from MP Biomedicals (USA). MTT Cell Proliferation and Cytotoxicity Assay Kit and ROS Assay Kit based on DCFH-DA were supplied by Beyotime Biotechnology Co. Ltd. (China). With the exception of mouse prostaglandin E2 (PGE₂) ELISA kit purchased from Cayman Chemical (USA), tumor necrosis factor (TNF)- α , interleukin (IL)-6 and IL-1 β ELISA kits were obtained from Neobioscience (China). Kits for molecules related to oxidative stress were purchased from BioAssay Systems (USA). All the other reagents are commercially available and used as received.

2.2. Synthesis and characterization of aromatized thioketal bond-bridged budesonide-tempol prodrugs (B-ATK-T)

2.2.1. Synthesis of 4-mercaptobutyric acid

4-mercaptobutyric acid was prepared according to the reference [42]. Briefly, 4-bromobutyric acid (8.24 g, 49.0 mmol) and thiourea (4.25 g, 53.5 mmol) were dissolved in 15 mL of ethanol and refluxed overnight. After removing the solvent by vacuum, 25 mL of aqueous NaOH (4 M, 100 mmol) was added. Then, the mixture is reacted under a nitrogen atmosphere at 90 °C for 16 h. After the reaction, the mixture was placed in an ice bath, and H₂SO₄ solution (2 M) was slowly added to the mixture to adjust the pH value to 2.0. The mixture was extracted 4 times with 60 mL of dichloromethane (DCM). The ethyl acetate phase produced by the reaction was combined. The organic layer was dried over anhydrous magnesium sulfate. The solvent was removed by vacuum distillation to give 4-mercaptobutyric acid as a colorless oil (8.6 g, 65.2%).

2.2.2. Synthesis of aromatized thioketal (ATK)

The aromatized thioketal (ATK) based on 4-mercaptobutyric acid is synthesized by the method previously reported with modification [43]. A solution of 9-fluorenone (0.50 g, 2.77 mmol) and 4-mercaptobutyric acid (0.57 mL, 5.54 mmol) in dichloromethane (3.0 mL) was added in TFA (0.85 mL, 1.11 mmol) and stirred at room temperature for 12 h. The reaction solution was poured into a saturated NaHCO₃ solution, and a large amount of precipitate appeared upon stirring. After filtration, the collected precipitate was washed 3 times with dd H₂O, and dried under vacuum at 45 °C for 12 h. The crude product was recrystallized from methanol to give a pale-yellow crystal, which is ATK (0.94 g, 80.7%).

2.2.3. Synthesis of budesonide-ATK (B-ATK)

Under the protection of N₂, budesonide (0.430 g, 1 mmol), DMAP (0.024 g, 0.2 mmol) and ATK (0.402 g, 1 mmol) were dissolved in anhydrous DCM. 0.412 g dicyclohexylcarbodiimide (DCC) was dissolved in 5 mL of anhydrous DCM and slowly added dropwise to the above mixed solution (ice-water bath). After stirring at room temperature for 48 h, the filtrate was concentrated. The filtrate was added dropwise to ice-cold anhydrous diethyl ether. Then, the obtained precipitate was dissolved in anhydrous DCM and poured into a large amount of cold anhydrous diethyl ether to give B-ATK (0.589 g, 72.3%).

2.2.4. Synthesis of Janus-prodrug budesonide-ATK-tempol (B-ATK-T)

Tempol (0.086 g, 0.5 mmol), DMAP (0.012 g, 0.1 mmol) and B-ATK (0.407 g, 0.5 mmol) were dissolved in anhydrous DCM under a nitrogen atmosphere. 5 mL DCM solution containing 0.206 g of DCC was slowly added dropwise to the above solution under ice bath. After 48 h, the filtrate was obtained by filtration, then poured into cold anhydrous diethyl ether. The precipitate was vacuum dried to obtain the final product B-ATK-T (0.316 g, 65.2%).

2.2.5. Synthesis of control prodrug budesonide-TK-tempol (B-TK-T)

According to the above procedure, only 9-fluorenone was replaced by acetone to obtain a white

solid B-TK-T (overall yield 46.6%).

2.2.6. Compound characterization

¹H NMR spectra were acquired using an Agilent DD2 600 MHz NMR spectrometer. Matrix-assisted laser desorption/ionization time-of-flight mass spectrometry (MALDI-TOF MS) was conducted on a MALDI-7090 TOF-TOF mass spectrometer (Shimadzu). Electrospray ionization mass spectrometry (ESI-MS) was conducted using an ESI-Triple Quad mass spectrometer (Bruker).

2.3. Preparation of B-ATK-T NP and Bud/Tem co-loaded PLGA NP

Benefiting from the amphiphilic property of B-ATK-T, prodrug nano-assemblies B-ATK-T NP were prepared by modified one-pot nano-precipitation method [44]. Briefly, 30 mg B-ATK-T Janus-prodrug was dissolved in 2 mL acetonitrile and then added dropwise into 8 mL deionized water containing 4 mg lecithin and 8 mg DSPE-PEG_{2K} under stirring. Self-assemblies of B-ATK-T occurred spontaneously. After 2 h, the residual acetonitrile was removed by vacuum distillation. To prepare dye-labeled B-ATK-T NP, DiI was co-dissolved with B-ATK-T in acetonitrile and then added dropwise into water with lecithin and DSPE-PEG_{2K}. The reaction solution was further placed in a dialysis bag (MWCO: 1000 Da), dialyzed against water for 48 h to remove unassembled B-ATK-T and dye. After that, NPs were collected and lyophilized.

In order to compare with the carrier-assistant drug delivery system, Bud/Tem co-loaded PLGA nanoparticles (BT/PLGA NP) were prepared by the classical nanoprecipitation method. Briefly, 13.32 mg Bud, 5.33 mg Tem (equivalent to 30 mg B-ATK-T) and 30 mg PLGA were co-dissolved in 2 mL acetonitrile and added dropwise to 65 °C deionized water containing 4 mg lecithin and 8 mg DSPE-PEG_{2K}. The nanoparticles are formed under stirring. After dialysis and lyophilization, BT/PLGA NP was obtained.

2.4. Characterization of NPs

Dynamic light scattering (DLS) and ζ-potential measurements were performed on a Malvern Zetasizer Nano ZS Instrument at 25°C. Transmission electron microscopy (TEM) observation was carried out using a JEM-1400 microscope (JEOL, Japan).

To quantify the drug loading content in nanoparticles, 5 mg lyophilized B-ATK-T NP was completely hydrolyzed in acetonitrile with 1 mM H₂O₂, BT/PLGA NP was completely hydrolyzed in acetonitrile for extraction. The drug concentration was quantified by LC-MS. The detection wavelength for budesonide and tempol were 246 nm and 240 nm, respectively. For the determination of DiI, the same experiment was carried out using a fluorescence spectrophotometer (Ex/Em = 549 nm/565 nm). The concentrations of drugs were calculated according to their standard curves.

2.5. Critical aggregation concentration (CAC) measurements

The CAC of B-ATK-T was determined by DLS according to the method previously reported [45]. When the CAC is reached in solution, there is a sudden increase in intensity of scattered light due to the formation of nanostructures. A series of solutions of B-ATK-T ranging from 3×10^{-3} to 3×10^{-6} mg/mL were prepared from an aqueous stock solution of B-ATK-T at a concentration of 0.01 mg/mL. 0.4 μg/mL lecithin and 0.8 μg/mL DSPE-PEG were present in the assay system. The CAC was

estimated as the cross-point when extrapolating the intensity in the low and high concentration ranges. The measurements were repeated three times in order to check their reproducibility.

2.6. In Vitro evaluation of the ROS sensitivity and hydrolysis of B-ATK-T NP

To examine the sensitivity of B-ATK-T NP to different components of ROS, various ROS generators were prepared according to previous reports [46]. Aqueous solutions containing either H₂O₂ or OCl⁻ were prepared based on commercially available agents. Peroxynitrite (ONOO⁻) was obtained by the reaction of H₂O₂ and nitrite. Hydroxyl radical (•OH) was generated by the Fenton reaction between ferrous acetate and H₂O₂, while superoxide anion was produced by the xanthine-xanthine oxidase system. Briefly, B-ATK-T NP at 1.0 mg/mL were separately incubated 3 mL medium with or without different ROS for 12 h, the hydrolysis degree was subsequently measured by UV-vis spectroscopy at 500 nm.

The hydrolysis behavior of B-ATK-T NP (1.0 mg/mL) was examined in 3 mL of PBS (10 mM, pH 7.4) containing various concentrations (0, 0.05, 0.1, 0.25, 0.5, 1 mM) of H₂O₂ at 37 °C. Quantitative experiments were conducted by measuring the absorbance of NP-containing aqueous solutions at 500 nm after incubation for various periods of time (0, 5, 10, 15, 20, 25, 30, 40, 60, 80, 120, 180, 240, and 300 min). Similarly, hydrolysis of B-ATK-T NP in buffer solutions with or without 1 mM H₂O₂ was studied at different pH (varying from pH 1.2, 7.4 to 9.0).

Meanwhile, simulated gastric fluid (50 mL of PBS containing 0.16 g pepsin, 0.1 g NaCl, 0.35 mL of 38% HCl solution) and simulated intestinal fluid (50 mL of PBS with 0.5 g trypsin, 0.34 g KH₂PO₄, and 76 mg NaOH) were prepared. Hydrolysis profiles, hydrodynamic diameter and polydispersity index (PDI) of B-ATK-T NP were tested in the gastrointestinal fluid environment. Also, size distribution and ζ-potential of B-ATK-T NP in PBS, 10% FBS or two simulated gastrointestinal fluids were determined.

In addition, the morphology of B-ATK-T NP with or without 1 mM H₂O₂ treatment was observed by TEM, and the particle size distribution was determined by DLS.

2.7. Drug release of B-ATK-T NP

To verify the responsive hydrolysis process and the hydrolysate, 60 mg of B-ATK-T was incubated in 1.0 mM H₂O₂ for 24 h, and the suspension was subjected to ESI-MS spectrometry. Mass spectrometry was performed using positive ion mode.

In another parallel experiment, 1 mL of newly prepared B-ATK-T NP suspension was put into a dialysis membrane (MWCO: 1000 Da), which was immersed into 40 mL PBS with or without different concentrations (0, 1, 5, 25, 50, 100 mM) of H₂O₂ for various times (0, 5, 10, 15, 20, 25, 30, 40, 60, 80, 120, 180, 240, and 300 min), and 4.0 mL of the supernatant was withdrawn. The amount of components released was determined by LC-MS.

2.8. Cytotoxicity evaluation by MTT assay

RAW264.7 cells were cultured in DMEM medium supplemented with 10% (v/v) FBS, 100 U/mL of penicillin, and 100 µg/mL of streptomycin in a 5% CO₂ humidified environment at 37 °C. For the methyl thiazolyl tetrazolium (MTT) assay, cells were planted at 1×10^4 cells/well in 96-well plates for 24 h before B-ATK-T NP or Bud or Tem were added. Subsequently, cells were treated with the

medium containing NP or drug at various concentrations (varying from 0, 7.8, 31.25, 125, 500, 1000 µg/mL) for 12 h. The cell viability was quantified by the MTT assay.

2.9. Intracellular uptake and drug release of B-ATK-T NP in RAW264.7 cells

RAW264.7 cells were seeded in 12-well plates at a density of 2×10^5 cells/well in 1 mL of growth medium. After 24 h, the culture medium was replaced with 1 mL of fresh medium containing 5 µg/mL DiI-labeled B-ATK-T NP and incubated for various periods of time (0.5, 1, 2, 4, and 8 h). Then, the cells were digested and fluorescence intensity was determined using a flow cytometer (BD Accuri C6). Through similar procedures, dose-dependent (1.25, 2.5, 5, 10, and 20 µg/mL DiI/B-ATK-T NP) internalization profiles were examined after 1 h of incubation.

Meanwhile, the drug release of B-ATK-T NP or BT/PLGA NP in cells were examined by a parallel test. Various concentrations of B-ATK-T NP or BT/PLGA NP were incubated with RAW264.7 cells for 1 h. After that, replaced with fresh medium, the cells were digested and acetonitrile was added to extract the drugs. The content of Bud and Tem were analyzed by LC-MS. The mobile phase was 70% acetonitrile and the flow rate was 0.5 mL/min.

In order to further verify the drug release of B-ATK-T NP in response to oxidative stress, RAW264.7 cells were incubated with proinflammatory phorbol-12-myristate-13-acetate (PMA, 100 ng/mL) and 20 µg/mL B-ATK-T NP for 8 h, and the intracellular drug concentration was determined according to the same method.

2.10. In Vitro biological activity of B-ATK-T NP

2.10.1. Anti-oxidative and anti-inflammatory activity of B-ATK-T NP in RAW264.7 cells

Murine macrophage RAW264.7 cells (2×10^5 cells/well) were cultured in 12-well plates with culture medium (DMEM, 10 wt% FBS, 1 wt% penicillin-streptomycin solution) for 12 h. Then fresh medium was changed and cell were cultured in the presence of 100 ng/mL PMA with 20 µg/mL B-ATK-T NP or equivalent Bud and Tem (8.25 µg/mL Bud and 3.11 µg/mL Tem) for 1 h. Subsequently, cells were washed three times with Hank's balanced salt solution (HBSS) and treated with 10 µM DCFH-DA in the dark at 37 °C for 40 min. Cells were washed thrice with HBSS and fixed by 4 wt % paraformaldehyde for 30 min at room temperature. The coverslips were fixed and mounted, and fluorescence microscopy images were acquired (BX51TRF, Olympus). Quantitative analyses were conducted by flow cytometry assay. RAW264.7 cells were cultured in 12-well plates as aforementioned. Cells were then treated with 10 µM DCFH-DA in the dark at 37 °C for 40 min. After the collected cells were washed thrice by HBSS, fluorescent intensities were measured by flow cytometer (Accuri C6, BD).

For the determination of inflammatory factors, follow the experimental procedure described above. After culture media were collected, the levels of inflammatory cytokines including tumor necrosis factor- α (TNF- α) and interleukin-6 (IL-6) were determined by ELISA kits (Neobioscience) according to the manufacturer's instructions.

2.10.2. Anti-apoptotic activity of B-ATK-T NP in RAW264.7 cells

Apoptosis analysis was conducted using FITC Annexin V Apoptosis Detection Kit with 7-AAD according to the manufacture's protocol. Specifically, RAW264.7 cells were seeded in a 6-well plate

at 2×10^5 cells/well and incubated overnight. The medium was then replaced with fresh growth medium containing 20 $\mu\text{g}/\text{mL}$ B-ATK-T NP or 8.25 $\mu\text{g}/\text{mL}$ Bud plus 3.11 $\mu\text{g}/\text{mL}$ Tem. After 2 h of incubation, cells were treated with 200 μM H_2O_2 for 8 h. Then, cells were washed with cold BioLegend's cell staining buffer, digested with 0.25 wt % trypsin, and collected by centrifugation. After the cells were resuspended in 100 μL of Annexin V binding buffer with 2.5 μL of Annexin V and 5 μL of 7-AAD viability staining solution at 1×10^5 cells/mL, they were vortexed gently and incubated in a dark room for 15 min. Finally, 400 μL of Annexin V binding buffer was added for analysis by flow cytometry (Accuri C6, BD).

2.11. Animals

All animal experiments were performed in accordance with the Guide for the Care and Use of Laboratory Animals proposed by the National Institutes of Health. All procedures and protocols were approved by the Animal Ethics Committee at Southwest University. C57BL/6 mice (18-20 g) were obtained from the Institute of Experimental Animals, Chongqing Institute of Chinese Materia Medica. Animals were housed in standard mouse cages under conditions of optimum light, temperature, and humidity, with *ad libitum* access to water and food. Before further experiments were performed, all mice were acclimatized for at least 7 days.

2.12. In Vivo pharmacokinetic study

According to the previously described protocols [47], ulcerative colitis in mice was induced by the drinking water containing 3% (w/v) DSS for 7 days. At the day 7, mice were single oral administration 400 μL of B-ATK-T NP (200 $\mu\text{g}/\text{mL}$) or 82.5 $\mu\text{g}/\text{mL}$ Bud with 31.1 $\mu\text{g}/\text{mL}$ Tem (equal to 200 $\mu\text{g}/\text{mL}$ B-ATK-T NP). At predefined time points (0.25, 0.5, 0.75, 1, 1.25, 1.5, 1.75, 2, 3, 4, 6, 8, 12, 16 and 24 h), blood samples and colonic tissues were collected. The whole blood samples were immediately centrifuged at 12,000 g for 2 min to obtain plasma. Then 800 μL of ice-cold methanol was added into 200 μL of plasma to precipitate protein. After centrifugation at 12,000 g for 2 min, the supernatant was purged with nitrogen, reconstituted with methanol, and detected by LC-MS. The mobile phase was consisted of acetonitrile and water at 70:30 (v/v). To determine the drug distribution in colon, the colonic tissues were homogenized and centrifuged. Bud and Tem in the supernatant were extracted with acetonitrile. Quantification was also performed by LC-MS. Typical pharmacokinetic parameters such as the maximum plasma/colon concentration (C_{max}), time to reach C_{max} (T_{max}), and the area under the plasma/colon drug concentration-time curve (AUC) were calculated.

2.13. In Vivo efficacies of B-ATK-T NP in colitis mice

According to the aforementioned procedures, the mouse model of colitis was established by induction with DSS (3% w/v). Mice were divided into four groups: the DSS group (DSS induced mice without treatment); the Bud + Tem free drugs group (DSS-induced mice oral administered with 82.5 $\mu\text{g}/\text{mL}$ Bud plus 31.1 $\mu\text{g}/\text{mL}$ Tem daily); the B-ATK-T NP group (DSS-induced mice oral administered daily with 400 μL 200 $\mu\text{g}/\text{mL}$ B-ATK-T NP); the normal control group (healthy mice without DSS).

2.13.1. Evaluation on the degree of colitis

During the whole period of treatment, changes in the body weight, visible stool consistency, and

fecal bleeding were assessed each day. Disease activity index (DAI) is defined as the summation of the stool consistency index (0-3), fecal bleeding index (0-3), and weight loss index (0-4) [47].

2.13.2. Histological assessments

After various treatments, mice were euthanized and the entire colon (from the cecum to the rectum) was collected. The colonic length was measured and gently washed with saline. Then, 1 cm of the distal section was used for histological assessment. The distal colon was fixed in 4% (v/v) buffered formalin for 1 day before paraffin embedding. Then, 7 μm thick sections of the distal colon were prepared and stained with hematoxylin and eosin (H&E), followed by imaging with optical microscopy.

Histological sections were scored as described previously [48]. For the epithelium (E), the standards are as follows: 0, normal morphology; 1, loss of goblet cells; 2, loss of goblet cells in large areas; 3, loss of crypts; and 4, loss of crypts in large areas. For the infiltration (I), it was evaluated by the following standard scores: 0, no infiltrate; 1, infiltrate around the crypt basis; 2, infiltrate reaching the muscularis mucosae; 3, extensive infiltration reaching the muscularis mucosae and thickening of the mucosa with abundant edema; and 4, infiltration of the submucosa. The total histological score was presented as E + I.

2.13.3. Quantification of pro-inflammatory cytokines, and oxidative mediators in the colonic tissues

The remaining colon section was used to measure the levels of tumor necrosis factor- α (TNF- α), prostaglandin E₂ (PGE₂), interleukin-1 β (IL-1 β), malondialdehyde (MDA) and H₂O₂. Briefly, the colonic tissues were isolated from mice after different treatments, and they were homogenized in ice-cold potassium phosphate buffer (pH 6.0) containing 0.5% hexadecyltrimethylammonium bromide. The homogenates were sonicated, freeze-thawed 3 times, and centrifuged at 10,621 g at 4 °C for 15 min. The levels of PGE₂, TNF- α and IL-1 β in the supernatant were determined using the corresponding detection kits. To quantify the level of H₂O₂, 100 mL of supernatant from the tissue homogenate was mixed with 1 mL of aqueous solution of molybdic acid (2.4 mmol/mL) that was preheated at 37 °C. After the mixture was incubated for 1 min, 1 mL of the termination reagent was added. Then the complex formed by H₂O₂ and molybdic acid was measured at 405 nm, and the concentration of H₂O₂ was calculated. The level of MDA in the supernatant of homogenate was quantified by using QuantiChrom TBARS assay kit.

2.14. Effect of B-ATK-T NP on survival rate of colitis mice

Mice were treated with 3% DSS, and from the 5th day, 200 $\mu\text{g}/\text{mL}$ B-ATK-T NP or equivalent Bud + Tem were orally administered each day until any group has no surviving mice (n = 10 in each group). The survival rate was recorded at the same time on each day (8:00 pm).

2.15. Safety evaluation of B-ATK-T NP

Male C57BL/6 mice were randomly divided into two groups (n = 5). B-ATK-T NP in PBS was orally administered at 200 $\mu\text{g}/\text{mL}$ for 400 μL . After one week, animals were euthanized and blood samples were collected for hematological analysis and quantification of biochemical markers relevant to liver/kidney functions. Major organs including heart, liver, spleen, lung, and kidney were isolated. Histopathological sections were prepared and stained with H&E.

2.16. Statistical Analysis

Data are expressed as mean \pm standard deviation (SD). Statistical analysis was assessed using one-way ANOVA test. A value of $p < 0.05$ was considered statistically significant.

3. Results and discussion

3.1. Synthesis and characterization of Janus-prodrug B-ATK-T

The synthetic route of Janus-prodrug B-ATK-T based on aromatized thioketal (ATK) was shown in **Figure 2**. The first step is preparation of linker ATK. Briefly, 4-bromobutyric acid was reacted with thiourea to obtain 4-mercaptobutyric acid (yield 53.2%). ^1H NMR of 4-mercaptobutyric acid (600 MHz, CDCl_3) δ 1.24-1.40 (t, 2H, $\text{HOOC-CH}_2\text{-CH}_2\text{-CH}_2\text{-SH}$), 1.89-2.00 (t, 2H, $\text{HOOC-CH}_2\text{-CH}_2\text{-CH}_2\text{-SH}$), 2.51-2.65 (t, 2H, $\text{HOOC-CH}_2\text{-CH}_2\text{-CH}_2\text{-SH}$), 10.40 (s, H, $\text{HOOC-CH}_2\text{-CH}_2\text{-CH}_2\text{-SH}$). ESI-MS m/z : calculated for $\text{C}_4\text{H}_8\text{O}_2\text{S}$ $[\text{M}+\text{H}]^+$ 121.17, found: 121.3. (Data are not shown). Then, under the catalysis of TFA, two 4-mercaptobutyric acids were reacted with a 9-fluorenone to form an ATK (yield 80.7%) with a dicarboxylic structure. ^1H NMR of ATK (600 MHz, $\text{CD}_3\text{OD-d}_4$) δ 7.62-7.60 (d, 2H, Ar-H), 7.59-7.55 (d, 2H, Ar-H), 7.54-7.50 (t, 2H, Ar-H), 7.35-7.27 (t, 2H, Ar-H), 2.75-2.69 (t, 4H, $-\text{OOC-CH}_2\text{-CH}_2\text{-CH}_2\text{-S-}$), 2.45-2.38 (t, 4H, $-\text{OOC-CH}_2\text{-CH}_2\text{-CH}_2\text{-S-}$), 2.05-1.94 (m, 4H, $-\text{OOC-CH}_2\text{-CH}_2\text{-CH}_2\text{-S-}$). MALDI-TOF-MS m/z : calculated for ATK ($\text{C}_{21}\text{H}_{22}\text{O}_4\text{S}_2$) $[\text{M}+\text{H}]^+$ 403.096, found: 403.521 (**Figure S1-S2**).

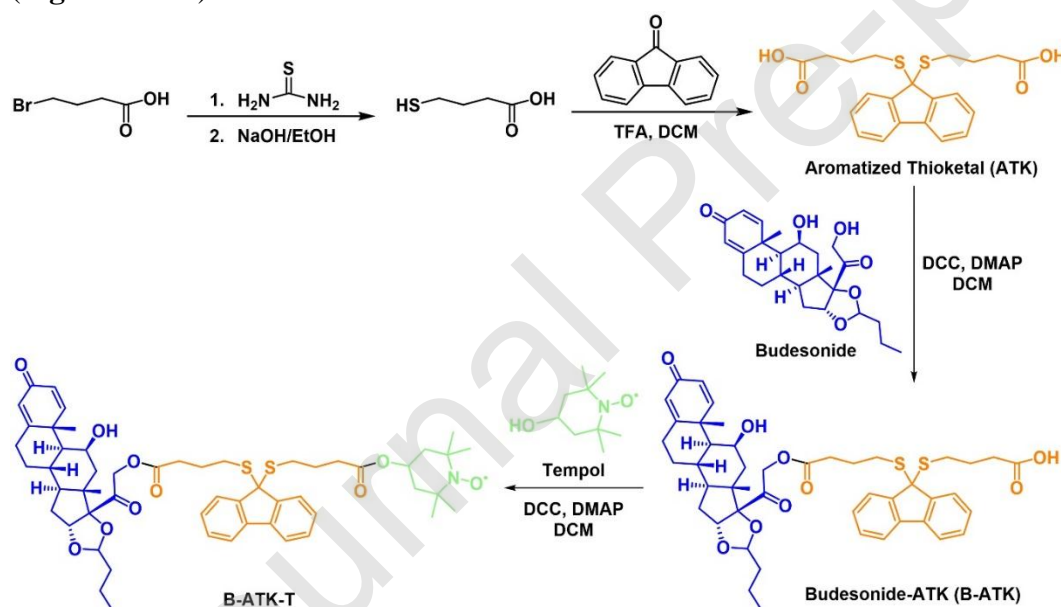


Figure 2. The synthetic route of the designed aromatized thioketal bond-bridged budesonide-tempol prodrug (B-ATK-T).

In the second step, the hydroxyl group of Bud formed an ester bond with one carboxyl group of ATK under the catalysis of DCC/DMAP to obtain Bud-ATK (B-ATK), yield 72.3%. ^1H NMR of B-ATK (600 MHz, $\text{CD}_3\text{OD-d}_4$) δ 7.62-7.59 (d, 2H, Ar-H), 7.58-7.55 (d, 2H, Ar-H), 7.53-7.48 (t, 2H, Ar-H), 7.44-7.39 (dd, 1H, $-\text{CO-CH=CH-CH-C=CH-}$), 7.32-7.28 (t, 2H, Ar-H), 6.25-6.20 (d, 1H, $-\text{CO-CH=CH-CH-C=CH-}$), 6.00-5.60 (d, 1H, $-\text{CO-CH=CH-CH-C=CH-}$), 2.75-2.69 (t, 4H, $-\text{OOC-CH}_2\text{-CH}_2\text{-CH}_2\text{-S-}$), 2.43-2.36 (t, 4H, $-\text{OOC-CH}_2\text{-CH}_2\text{-CH}_2\text{-S-}$), 2.00-1.93 (m, 4H, $-\text{OOC-CH}_2\text{-CH}_2\text{-CH}_2\text{-S-}$). MALDI-TOF-MS m/z : calculated for B-ATK ($\text{C}_{46}\text{H}_{54}\text{O}_9\text{S}_2$) $[\text{M}+\text{H}]^+$ 815.324, found: 815.103

(**Figure S3-S4**). Then, Tem was coupled to the other carboxyl group of B-ATK to form an ester bond, obtaining Janus-prodrug B-ATK-T (yield 65.2%). Since Tem is paramagnetic that make it difficult to obtain the ^1H NMR signal, B-ATK-T was confirmed by MALDI-TOF-MS (**Figure S5**). MALDI-TOF-MS m/z : calculated for B-ATK-T ($\text{C}_{55}\text{H}_{70}\text{NO}_{10}\text{S}_2$) $[\text{M}+\text{H}]^+$ 969.44, found: 969.603.

Following the similar method, non-aromatized B-TK-T was synthesized as control. In the method above, 9-fluorenone was replaced by acetone to obtain TK. And the subsequent steps were kept unchanged, giving a white solid B-TK-T (overall yield 46.6%, **Figure S6**). MALDI-TOF-MS m/z : calculated for B-TK-T ($\text{C}_{45}\text{H}_{68}\text{NO}_{10}\text{S}_2$) $[\text{M}+\text{H}]^+$ 847.428, found: 847.418. All these results demonstrated that both B-ATK-T and B-TK-T were successfully synthesized.

3.2. Preparation and characterization of B-ATK-T NP

Janus-prodrug nano-assemblies B-ATK-T NP were prepared by modified nanoprecipitation method [44]. It is critical to keep nano-formulated prodrug with high stability, even at very low concentrations in the case of intense dilution of the physiological fluids. Critical aggregation concentration (CAC) is regarded as a key evidence for the nano-aggregates forming ability [49]. The CAC of B-ATK-T was determined by DLS based on the sudden change in the scatter light intensity when the nanostructures are formed [45]. As shown in **Figure 3A**, at concentrations below the CAC, the detected scattering intensity of the nanoparticles is approximately equal to the constant value corresponding to the deionized water. As the number of B-ATK-T in the solution increases, the intensity begins to increase linearly. The CAC of B-ATK-T NP obtained from the intersection of the best fit lines drawn by the data points was about 0.16 $\mu\text{g}/\text{mL}$ in aqueous solution containing lection and DSPE-PEG. The relatively low CAC of B-ATK-T NP indicates that it is very easy to form nanostructures in aqueous solution and remain stable under strong dilution. However, the preparation of B-TK-T-based self-assemblies ended in failure. Even at a sufficiently large concentration of B-TK-T (up to 3 mg/mL), there was still no sharp increase in the intensity of the scattered light, and the CAC of B-TK-T cannot be measured (data not shown). The reason may be the lack of sufficient hydrophobicity of B-TK-T to form a stable colloidal system. This negative result revealed from another perspective that the ATK can bring more hydrophobic interactions between B-ATK-T molecules, and the potential π - π interactions between ATK and itself or drugs may also be one of the driving forces in the self-assembly process.

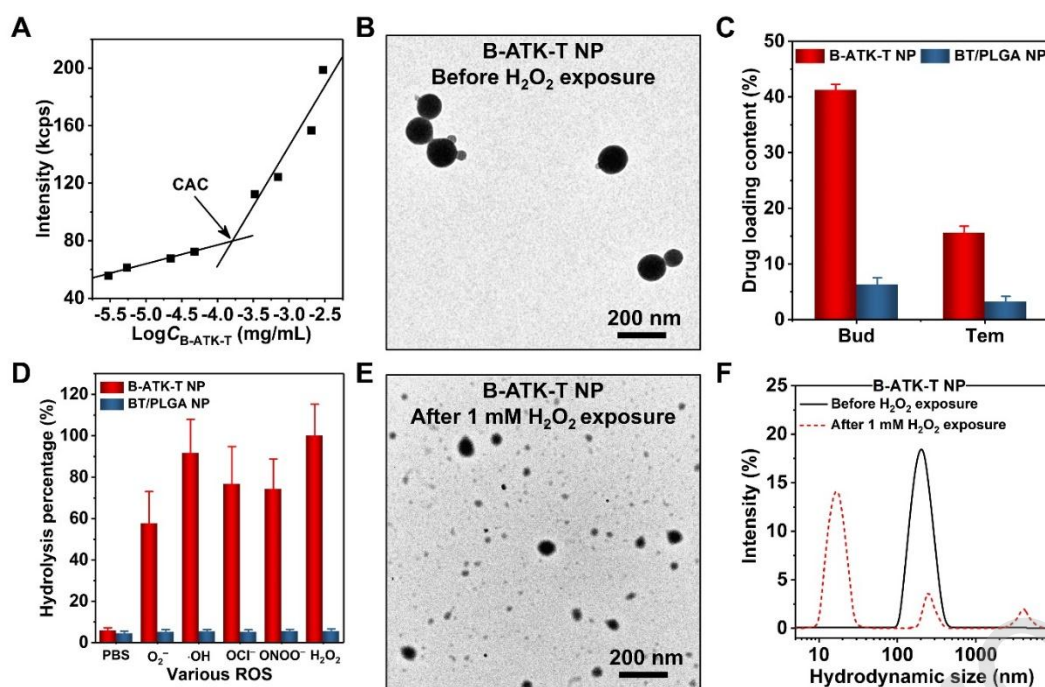


Figure 3. Preparation and characterization of B-ATK-T NP and BT/PLGA NP. **A**, The CAC of B-ATK-T determined by dynamic light scattering. **B**, TEM image of B-ATK-T NP. **C**, The drug loading content of Bud and Tem in B-ATK-T NP or BT/PLGA NP. **D**, Sensitivity of NP against various ROS. **E-F**, TEM image (**E**) and hydrodynamic size distributions (**F**) of B-ATK-T NP before and after 1 mM H₂O₂ exposure. All data are presented as mean ± SD (n = 6).

Characterization by TEM suggested that the as-prepared B-ATK-T NP exhibited a well-defined uniform spherical shape with an average size of approximate 100-120 nm (**Figure 3B**). In order to compare with the carrier-assistant drug delivery system, PLGA (an FDA-approved pharmaceutical polymer) was used as a carrier to co-load Bud and Tem to prepare BT/PLGA NP. The TEM image (**Figure S7A**) and size distribution (**Figure S7B**) proved that BT/PLGA NP has similar morphology with narrow size distribution to that of B-ATK-T NP. Since DSPE-PEG was used to enhance the colloidal stability, the peripheral PEG chains also introduce a negative potential for the BT/PLGA NP. According to the hydrodynamic diameter results from DLS, B-ATK-T NP and BT/PLGA NP maintained their particle size (**Figure S8A**) and low negative ζ -potential (**Figure S8B**) in 10% FBS for up to 48 h. These similar features of two NPs indicated that both of them have good compatibility in biological applications. Moreover, the drug loading content is a very important parameter for nano formulations. Interestingly, only 6.35% for Bud and 3.15 % for Tem were found in BT/PLGA NP, while Janus-prodrug B-ATK-T NP have significantly higher drug loading capacity (average 41.23% for Bud and 15.55% for Tem, w/w) (**Figure 3C**).

To sum up, the carrier-free nano-assemblies based on the Janus-prodrug B-ATK-T were successfully prepared by a simple one-step nanoprecipitation method. B-ATK-T NP has good colloidal stability and negative ζ -potential as BT/PLGA NP. Moreover, B-ATK-T NP was endowed higher drug loading capacity, leading to significantly improved drug-delivery efficiency and less excipient-associated toxicity.

3.3. ROS-responsive hydrolysis and drug release profiles of B-ATK-T NP

Is the built-in thioketal bond capable disassembling B-ATK-T NP to release the native drugs? The hydrolysis of B-ATK-T NP in PBS and PBS containing superoxide anion, hydroxyl radical, hypochlorite, peroxyxynitrite or hydrogen peroxide, respectively, were investigated. As depicted in **Figure 3D**, except for the absence of significant hydrolysis of B-ATK-T NP in PBS, other kinds of ROS resulted in disassembly of B-ATK-T NP. The hydrolysis percentage of B-ATK-T NP even reached nearly 100% when incubated with 1.0 mM H₂O₂. The non-selective ROS sensitivity of B-ATK-T NP endows them a wider range of applications. Of note, a comparable sized BT/PLGA NP showed no responsive hydrolysis under all examined conditions.

TEM image showed that B-ATK-T NP transformed to smaller particles as the regular globular morphology disappeared after incubation with 1.0 mM H₂O₂ for 12 h (**Figure 3E**). Consistent with the results of TEM, the particle size distribution of B-ATK-T NP changed significantly after H₂O₂ exposure. The hydrolysis triggered by 1.0 mM H₂O₂ caused that B-ATK-T NP disassembled and decomposed into small particles about 20 nm (**Figure 3F**). In addition, the effects of pH on the ROS-responsive hydrolysis of B-ATK-T NP were also investigated. Unlike other pH-dependent ROS responsive materials (such as boronate-based materials [50]), the hydrolysis performance of B-ATK-T NP in 1.0 mM H₂O₂ was not affected regardless of the pH (**Figure S9A**). In the absence of H₂O₂, B-ATK-T NP showed no significant hydrolysis in acidic, neutral or alkaline environment, indicating that B-ATK-T NP has good pH tolerance (**Figure S9B**).

In order to further investigate the ROS responsive hydrolysis mechanism, B-ATK-T was completely hydrolyzed in H₂O₂ and the hydrolyzed product was confirmed by ESI mass spectrometry (**Figure 4A**). The ESI MS spectrum showed the presence of molecular ion peak of γ -thiobutyrolactone ($[M+H]^+$ m/z , found: 103.50, calculated: 103.014), Tem ($[M+H]^+$ m/z , found: 173.10, calculated: 173.134), 9-fluorenone ($[M+H]^+$ m/z , found: 103.50, calculated: 103.014; $[M+Na]^+$ m/z , found: 203.20, calculated: 203.058), and Bud ($[M+H]^+$ m/z , found: 431.15, calculated: 430.236). Therefore, the hydrolysis process of B-ATK-T can be deduced as in **Figure 4B**. The thioketal bond was open when exposed to ROS, then 9-fluorenone, thiolated Bud and thiolated Tem were formed. Subsequently, the carbonyl carbon of thiolated product was attacked by its own thiol as a nucleophilic group. The ester bond was broken, thereby producing three small molecules of γ -thiobutyrolactone, Bud and Tem. These results demonstrated that B-ATK-T is capable of releasing native drugs by the triggering of H₂O₂.

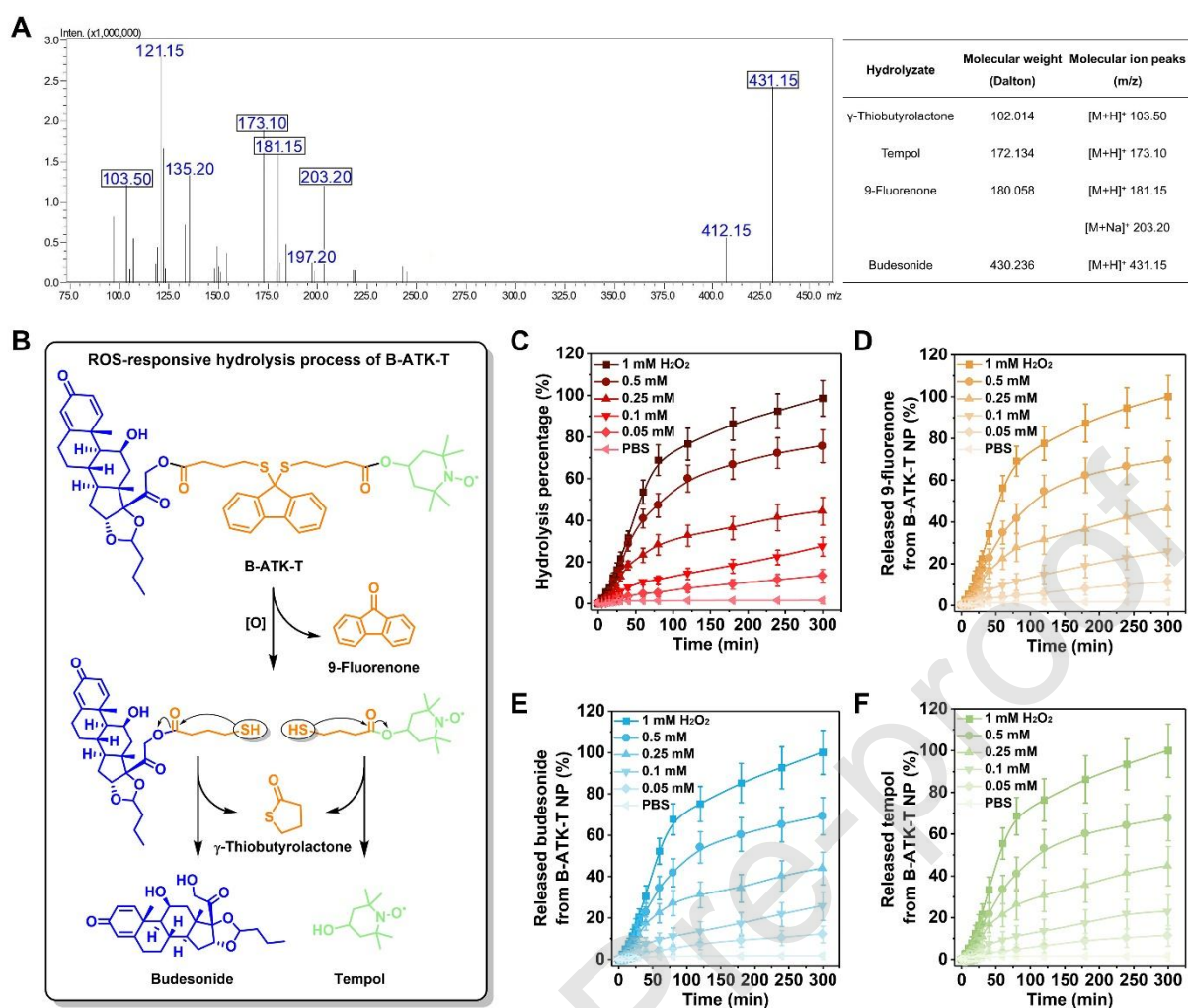


Figure 4. ROS-responsive hydrolysis process and drug release profiles of B-ATK-T NP. **A**, Mass spectrometric analysis of the hydrolysates of B-ATK-T in H_2O_2 . **B**, Schematic diagram of the ROS responsive hydrolysis process of B-ATK-T NP deduced from the experimental results. **C**, Hydrolytic profiles of B-ATK-T NP in 10 mM PBS with various concentrations of H_2O_2 . **D-F**, 9-fluorenone (**D**), budesonide (**E**) and tempol (**F**) release profiles of B-ATK-T NP in 10 mM PBS with various concentrations of H_2O_2 . All data are presented as mean \pm SD ($n = 6$).

The hydrolysis of B-ATK-T NP in media with different H_2O_2 concentrations were also investigated. From **Figure 4C**, the rapid and effective hydrolysis of B-ATK-T NP was observed at 0.25, 0.5 and 1.0 mM H_2O_2 , while only limited hydrolysis occurred at 0.1 or 0.05 mM H_2O_2 . In 1.0 mM H_2O_2 , the hydrolysis rate was close to 50% after 1 h. After 5 h, B-ATK-T NP was almost completely hydrolyzed. It is demonstrated that the responsive hydrolysis of B-ATK-T NP showed a H_2O_2 concentration dependence. 9-fluorenone (**Figure 4D**) and two therapeutic drugs (**Figure 4E-F**) release profiles of B-ATK-T NP at different H_2O_2 concentrations were measured by LC-MS. The release rate of the drugs and their cumulative release are also dependent on H_2O_2 concentration. Simultaneous release of drugs is critical for combination therapy. However, traditional drug co-loaded delivery system which contains two or more drugs, usually has different drug release rate due to the different hydrophilicity of drugs [51]. It is worth noting that the release characteristics of each molecule in B-ATK-T NP are approximately similar, which indicated two therapeutic drugs of B-ATK-T NP released like twins. In

summary, Janus-prodrug B-ATK-T NP was determined to be a broad ROS-sensitive self-assembled system for the treatment of inflammation-related diseases.

3.4. Biological effects of B-ATK-T NP in macrophages

Macrophages are involved in many cellular activities such as oxidative stress, inflammatory immune response, autophagy and so on [52]. They played an extremely important role in the pathogenesis of inflammatory diseases [53]. The cytotoxicity of Bud and Tem in murine macrophage RAW264.7 cells were examined. Both of them showed lower cytotoxicity and the cell survival rate remained above 90% (**Figure S10A-B**). Although the viability of RAW264.7 cells were gradually decreased with the increase dose of B-ATK-T NP after 12 h of incubation (**Figure S10C**), a relatively high cell viability of 82% could still be observed at a dose as high as 1000 $\mu\text{g/mL}$. The reason for the slight decrease in cell viability may be the high concentration of NPs absorbed on the cell surface, causing a physical barrier on the cell surface, thereby inhibiting cell proliferation [54]. These data suggested that B-ATK-T NP displayed low toxicity in RAW264.7 cells.

Flow cytometry and LC-MS were performed to investigate the uptake behavior of B-ATK-T NP by RAW264.7 cells using DiI-labeled B-ATK-T NP. With prolonged incubation, internalized DiI/B-ATK-T NP notably increased (**Figure S11A-B**). In dose-dependent experiments, flow cytometry analysis showed enhanced endocytosis of DiI/B-ATK-T NP in RAW264.7 cells with increased dose (**Figure S11C-D**). In addition, it is important to know whether internalizations indiscriminately hydrolyze B-ATK-T NP and release the drugs. LC-MS was used to detect the intracellular drug content after incubating 20 $\mu\text{g/mL}$ B-ATK-T NP or BT/PLGA NP with the resting state cells for different time. As shown in **Figure S12A**, B-ATK-T NP leaked a very small amount of Bud and Tem at the beginning of contact with cells, with the leakage only about $1.4 \pm 0.7\%$ and $0.5 \pm 0.4\%$, respectively. As time went on, no significant increasing leakage was observed. In contrast, the initial leakage of BT/PLGA NP after incubation with cells was lower. But the leak rate was gradually increased (**Figure S12B**). Such results indicated that the Janus-prodrug B-ATK-T NP is more stably presented in the rest macrophage cells than the conventional carrier like PLGA.

What about the performance of B-ATK-T NP in a stressful macrophage? After the RAW264.7 cells were transformed into inflammatory cells by the classical proinflammatory substance phorbol-12-myristate-13-acetate (PMA), 20 $\mu\text{g/mL}$ B-ATK-T NP or BT/PLGA NP was incubated with the cells for 8 h. From **Figure 5A**, two therapeutic drugs in B-ATK-T NP have been almost completely released ($98.8 \pm 0.1\%$ for Bud, $97.9 \pm 0.4\%$ for Tem), while only $43.7 \pm 6.6\%$ Bud and $18.2 \pm 6.4\%$ Tem released from BT/PLGA NP. Such a dramatic difference is due to the ROS-responsiveness of the B-ATK-T NP. In view of non-sensitive BT/PLGA NP having slow drug release rate, it will not be further discussed in subsequent experiments and replaced by the combination of equivalent Bud and Tem.

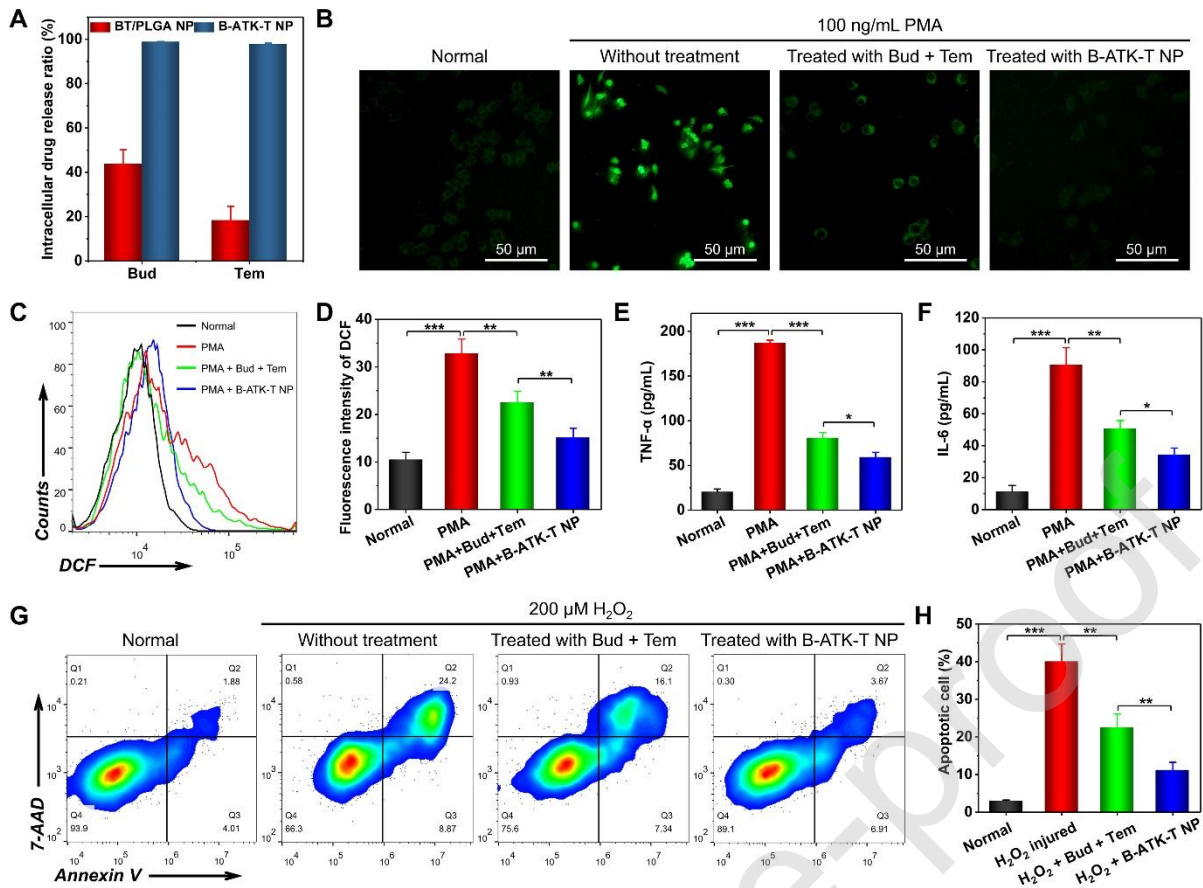


Figure 5. In vitro anti-oxidative stress, anti-inflammatory activity and anti-apoptosis of B-ATK-T NP in RAW264.7 cells. **A**, Intracellular drug release of B-ATK-T NP or BT/PLGA NP in RAW264.7 cells stimulated by the proinflammatory substance PMA. **B**, Fluorescence microscopy images showing the intracellular generation of ROS in cells stimulated with 100 ng/mL of PMA and B-ATK-T NP at 20 μg/mL for 1 h. Meanwhile, 8.25 μg/mL Bud and 3.11 μg/mL Tem were administered as a comparison group according to the drug loading content of B-ATK-T NP. Without treatment group as a control group. DCFH-DA was used as an intracellular ROS probe. **C-D**, Typical flow cytometry profiles (**C**) and quantitative analysis (**D**) of fluorescence intensity of DCF in cells. **E-F**, Inhibition of the expression of typical inflammatory chemokines like TNF-α (**E**) and IL-6 (**F**). For **B-F**, before analysis, cells were treated under the same conditions. **G-H**, Representative flow cytometry profiles (**G**) and quantitative data (**H**) of cell apoptosis. RAW264.7 cells were incubated with 20 μg/mL B-ATK-T NP or equivalent Bud + Tem against 200 μM H₂O₂ for 6 h, apoptotic cells were determined by staining with Annexin V and 7-AAD. All data are presented as mean ± SD (n = 6). *p < 0.05, **p < 0.01, ***p < 0.001.

Fluorescence microscopy was used to measure the anti-oxidative effects of B-ATK-T in RAW264.7 cells with DCFH-DA as ROS probe. It can be seen that the level of intracellular ROS in RAW264.7 cells significantly increased by stimulated with 100 ng/mL PMA, whereas treated with 20 μg/mL B-ATK-T NP significantly reduced ROS generation (**Figure 5B**). This finding was further confirmed by quantitative analysis of flow cytometry. **Figure 5C-D** showed that PMA caused a 3.1-fold intracellular ROS levels compared with resting state cells. Meanwhile, B-ATK-T NP decreased it to 1.4-fold, while the equivalent Bud + Tem treatment (8.25 μg/mL Bud and 3.11 μg/mL Tem) only reduced it to 2.2-fold. B-ATK-T NP could dramatically inhibit the PMA-induced oxidative stress, as

well as the expression of inflammatory cytokines in RAW264.7 cells, including TNF- α and IL-6 (**Figure 5E-F**). Thus, B-ATK-T NP has a better anti-inflammatory effect than the combination of the two drugs ($p < 0.05$).

High concentrations of H₂O₂ would cause cell oxidative stress outbreaks and excessive inflammatory immune responses, leading to apoptosis [55]. The cells stained with Annexin V (Annexin V⁺/7-AAD⁻) were considered to be early apoptotic cells, while stained with 7-AAD (Annexin V⁺/7-AAD⁺) were considered to be severe necrotic cells. In this study, injured by 200 μ M H₂O₂ for 6 h, the proportion of apoptotic cells was as high as nearly 40%. Treatment with 20 μ g/mL B-ATK-T NP dropped it significantly to about 11.1%. Meanwhile, the equivalent drugs could only reduce this ratio to around 22.4% (**Figure 5G-H**).

These results of the cell experiments demonstrated that the biocompatible B-ATK-T NP could achieve sufficient uptake, rapid hydrolysis and complete drug release in inflammatory macrophages due to its ROS-responsive property. This is the basis for B-ATK-T NP to achieve better anti-oxidation, anti-inflammation and anti-apoptosis effects than the free drugs combination.

3.5. Application of B-ATK-T NP for targeted therapy of inflammatory bowel disease

It has been reported that the ROS level in intestinal of the patients with inflammatory bowel disease (IBD) is 10-100 times higher than that in normal people [56-58]. For treating IBD, oral administration is commonly regarded to be more convenient and acceptable than rectal administration. Although sulfasalazine (a prodrug form of the active ingredient 5-aminosalicylic acid) has been clinically applied by oral route [59], there is still a lack of research reports on dual-prodrugs. Based on the above findings, B-ATK-T NP was further investigated as a novel self-assembled Janus-prodrug for the treatment of IBD. As depicted in **Figure S13A**, after 4 h of incubation with simulated gastric or intestinal fluid, the particle size of B-ATK-T NP changed slightly with the similar trend in PBS. The maximum PDI of B-ATK-T NP were only 0.18 and 0.19, respectively (**Figure S13B**), which are less than 0.3 (the upper limit of the uniformity) [60]. This revealed that B-ATK-T NP could remain stable in harsh gastrointestinal environment. The selective accumulation of therapeutic drugs in colon is also important for effective therapy of IBD, especially for Bud and Tem which are easily absorbed into the blood. The pharmacokinetic and colon distribution profiles of Bud and Tem from B-ATK-T NP or free combination, were investigated in colitis mice induced by DSS (**Figure 6A**). B-ATK-T NP could significantly reduce the C_{max} of Bud and Tem in blood (**Figure S14A**), and also extended the time to reach C_{max} (T_{max}) from 2 h to 3 h (**Figure 6B**). Correspondingly, **Figure 6C** shows the cumulative amount of each drug in blood by calculating the area under the curve (AUC). B-ATK-T NP significantly reduced the amount of two drugs absorbed into blood. While in colon, B-ATK-T NP dramatically increased the C_{max} of the drugs (**Figure S14B**) and had no effect on T_{max} (4 h) compared to the free drugs group (**Figure 6D**). The concentration of two drugs of B-ATK-T NP in colon were 1.68 times and 1.65 times higher than that in free drugs group, respectively (**Figure 6E**). Although B-ATK-T NP may not significantly prolong the retention time of the drug in the colon, B-ATK-T NP can greatly increase the concentration of the drugs in the colon, thereby increasing the total amount of accumulated drugs in a certain period.

Compared to free drugs that are rapidly absorbed and metabolized in the gastrointestinal tract, the ROS-responsive Janus-prodrug B-ATK-T NP can effectively accumulate to the diseased colon tissue,

increase drug bioavailability and simultaneously decrease systemic exposure.

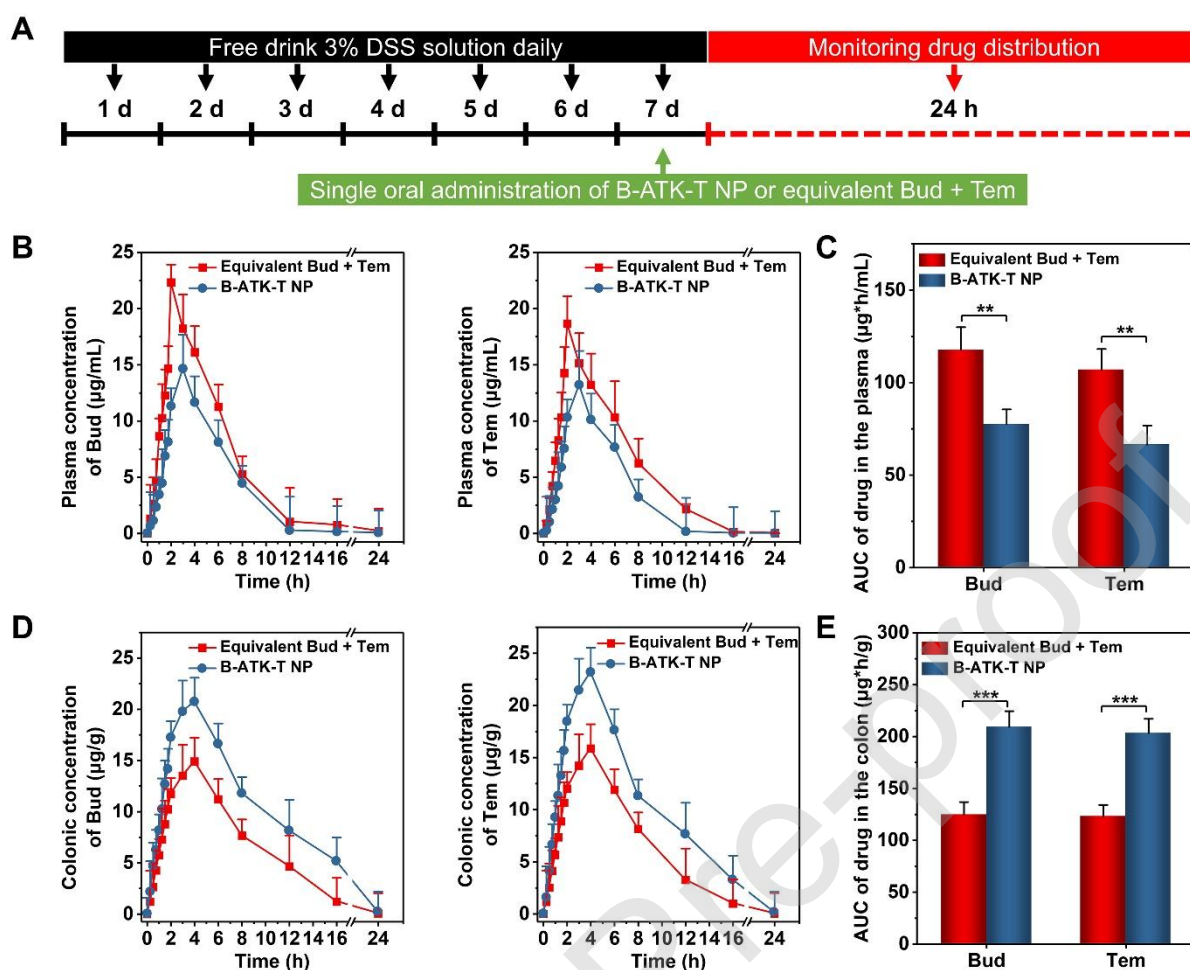


Figure 6. Selective accumulation of Bud and Tem from B-ATK-T NP in the colon of mice with DSS induced colitis. **A**, Establishment of colitis in mice by DSS induction and single oral administration 400 μL of 200 $\mu\text{g/mL}$ B-ATK-T NP or 82.5 $\mu\text{g/mL}$ Bud + 31.1 $\mu\text{g/mL}$ Tem (equal to 200 $\mu\text{g/mL}$ B-ATK-T NP) at 7th day. In the next 24 h, at the pre-determined time point, the blood and colon of the mice were collected for drug concentration monitoring. **B**, Quantitative analysis of Bud and Tem distribution in plasma. **C**, Cumulative amount of Bud and Tem in blood by calculating the area under the curve (AUC). **D-E**, the drug distribution (D) and cumulative amount of Bud and Tem in colon of colitis mice (E). All data are presented as mean \pm SD (n = 3). **p < 0.01, ***p < 0.001.

The anti-inflammation effects of B-ATK-T NP were finally investigated in colitis mice induced by DSS (**Figure 7A**). The body weight of normal mice maintained a slightly increase during the experiment, while the colitis mice began to show significant weight loss from day 3 (**Figure 7B**). Until day 7, the body weight loss was about 18%. Diseased mice relieved the trend of weight loss by daily oral administration of free drugs or B-ATK-T NP. Nevertheless, compared with the body weight loss about 10% in free drugs group, B-ATK-T NP was more effective that the final weight decreased by only about 4%. DSS-treated mice had significantly increased disease activity index (DAI) and shortened colon as compared to normal mice (**Figure 7C-D**). By contrast, B-ATK-T NP-treated mice displayed much lower DAI and notably preserved colonic length. From **Figure S15**, B-ATK-T NP also effectively increased stool consistency (decrease stool consistency index) and alleviated feces

bleeding (decrease feces bleeding index).

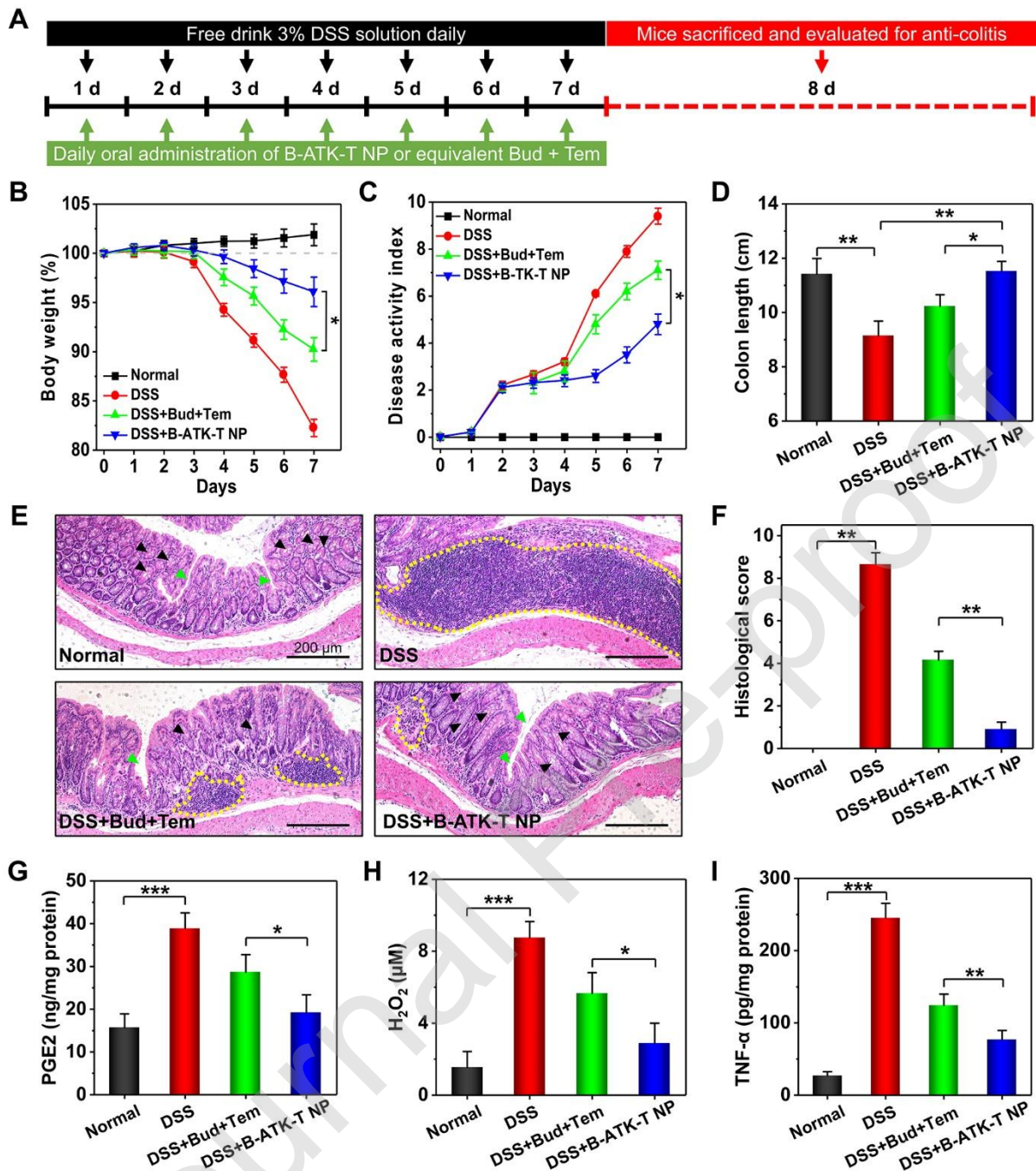


Figure 7. In vivo efficacies of B-ATK-T NP for treatment of colitis in mice. **A**, Establishment of DSS-induced colitis in mice and treatment regimens. Daily oral administration of 200 $\mu\text{g/mL}$ B-ATK-T NP or 82.46 $\mu\text{g/mL}$ Bud + 31.10 $\mu\text{g/mL}$ Tem (equal to 200 $\mu\text{g/mL}$ B-ATK-T NP). **B**, Changes in the body weight of mice during 7 days of treatment. **C**, Changes in DAI, which is the summation of the stool consistency index (0-3), fecal bleeding index (0-3), and weight loss index (0-4). **D**, The length of colonic tissues isolated from mice after 7 days of treatment. **E-F**, H&E stained histological sections (E) and histological score (F) of colonic tissues from mice subjected to various treatments. The area circled by the yellow line refers to the presence of inflammatory cell infiltration, the green arrow refers to the crypt structure, and the black arrow refers to the goblet cell. Scale bar represent 200 μm . **G-I**, The expression levels of representative factors of inflammation and oxidative stress

in colon. After 7 days of treatment, homogenates of the colonic tissues were prepared, and the concentrations of PGE-2 (G), H₂O₂ (H) and TNF- α (I) were separately measured by commercial kits. The total protein was measured by the BCA assay. All data are presented as mean \pm SD (n = 5). *p < 0.05, **p < 0.01, ***p < 0.001.

The examination of histological sections revealed serious necrocytosis, significantly loose goblet cell (black arrow), destruction of crypt (green arrow), as well as a high level of inflammatory cell infiltration (yellow circle) in the inflamed colon (**Figure 7E**). That is consistent with the histological scores reflected in **Figure 7F**. Bud + Tem free drugs treatment group still showed certain degrees of injuries in the colonic tissues. However, nearly normal histological microstructure was observed for B-ATK-T NP treated mice. It has been reported that mice with IBD usually have a certain degree of liver damage [61]. The abnormally increased level of alanine aminotransferase (ALT) was further detected. The level of ALT was mostly reversed by B-ATK-T NP treatment compared with the colitis mice, while the liver function of free drugs treated colitis mice is still affected (**Figure S16**). The existing report states that Bud nanosuspension can significantly reduce the number of macrophages and pro-IL-1 β expressing monocytes in colitis tissues [62]. It has also been reported that Tem can reduce the ratio of neutrophils in inflammatory tissues [63]. Therefore, B-ATK-T NP was speculated to reduce the number of inflammation-related cells.

To further investigate the mechanism of B-ATK-T NP alleviate colitis in mice, the expression levels of oxidative stress-related and pro-inflammatory mediators in colonic tissues were examined. It is known that Bud could reduce the production of lipid inflammatory mediators, such as prostaglandin E2 (PGE2) by inhibiting phospholipase A2 [64]. Tem, as a SOD mimic, could eliminate local overexpressed ROS and reduce correspondingly induced lipid peroxides, like MDA [16]. As depicted in **Figure 7G-I** and **Figure S17A-B**, the production of PGE2, H₂O₂, TNF- α , MDA and IL-1 β were all significantly up-regulated in the colon tissue of colitis mice. Benefiting from the targeted simultaneous release of Bud and Tem, B-ATK-T NP treatment had more significant efficacy than free drugs treatment in reducing the expression levels of PGE2, H₂O₂, TNF- α , MDA and IL-1 β . Moreover, the death of mice with colitis occurred from the 7th day, and within 15 days the survival rate decreased to 0 (**Figure S18**). On the 5th day, oral administration of 200 μ g/mL B-ATK-T NP daily delayed the initial death to the 10th day, and the survival rate on 15th day was 70%. Although mice with oral administration of free drugs occurred death also from the 10th day, the survival rate on the 15th day was only about 40%. This result fully demonstrates that B-ATK-T NP can effectively delay and reduce the death of mice induced by DSS on the basis of colitis relief.

In addition, oral administration of 400 μ L B-ATK-T NP (200 μ g/mL) showed high safety to blood and organ tissues, which proved a prerequisite for potential clinical transformation. Specifically, the number of red blood cells and white blood cells were not affected after the treatment. Liver and kidney function indicators represented by ALT and blood urea nitrogen (BUN) showed to be normal (**Figure S19**). H&E-stained sections and organ index also demonstrated that B-ATK-T NP did not cause pathological changes in all major organs of mice (**Figure S20**).

4. Conclusions

In summary, Janus-prodrug B-ATK-T NP was constructed to pursue the combined efficacy of the anti-inflammatory drug Bud and the anti-oxidative drug Tem. Driven by the hydrophobic interactions and π - π stacking interactions of aromatized thioketal, B-ATK-T can self-assemble to form regular

spherical nanostructures. Moreover, B-ATK-T NP was endowed high drug loading content with 41.23% of Bud and 15.55% of Tem, respectively, without the assist of any carrier. Unlike the simple co-administration of the free drugs, self-assembled B-ATK-T NP with extensive ROS sensitivity could release both Bud and Tem in a simultaneous and proportionate manner. In vitro studies have shown that B-ATK-T NP could exert excellent responsive release characteristics and the combined efficacy of anti-inflammation, anti-oxidation and anti-apoptosis in inflammatory cells. Strikingly, B-ATK-T NP can accumulate in DSS-induced inflamed mice colon, and effectively increase the maximum drugs concentration then avoid potential systemic side effects. B-ATK-T NP inhibited the expression of oxidative and proinflammatory mediators more excellently than free drugs, and also significantly reduced the death caused by IBD. In view of the ATK as a new ROS-responsive self-assembly platform, this work is expected to provide a new strategy for treatment of inflammatory diseases.

Data availability

The authors declare that all data supporting the findings of this study are available within the paper and its supplementary information, source data in this study are available from the online version.

Conflicts of interest

The authors declare no competing interests.

Acknowledgments

The work was supported by the Fundamental Research Funds for the Central Universities [SWU118123].

References

- [1] D.K. Podolsky, Inflammatory Bowel Disease, *New England Journal of Medicine*, 347 (2002) 417-429.
- [2] R. Hodson, Inflammatory bowel disease, *Nature*, 540 (2016) S97.
- [3] B. Khor, A. Gardet, R.J. Xavier, Genetics and pathogenesis of inflammatory bowel disease, *Nature*, 474 (2011) 307-317.
- [4] R.J. Xavier, D.K. Podolsky, Unravelling the pathogenesis of inflammatory bowel disease, *Nature*, 448 (2007) 427-434.
- [5] G.Y. Melmed, S.R. Targan, Future biologic targets for IBD: potentials and pitfalls, *Nat Rev Gastroenterol Hepatol*, 7 (2010) 110-117.
- [6] D.S. Pardi, Diagnosis and Management of Microscopic Colitis, *Am J Gastroenterol*, 112 (2017) 78-85.
- [7] S. Singh, J.D. Feuerstein, D.G. Binion, W.J. Tremaine, AGA Technical Review on the Management of Mild-to-Moderate Ulcerative Colitis, *Gastroenterology*, 156 (2019) 769-808.
- [8] S. O'Donnell, C.A. O'Morain, Therapeutic benefits of budesonide in gastroenterology, *Ther Adv Chronic Dis*, 1 (2010) 177-186.
- [9] A. Ryrfeldt, P. Andersson, S. Edsbacker, M. Tonnesson, D. Davies, R. Pauwels, Pharmacokinetics and metabolism of budesonide, a selective glucocorticoid, *Eur J Respir Dis Suppl*, 122 (1982) 86-95.
- [10] W. Rufle, P. Fruhmorgen, W. Huber, J.M. Kimmig, Budesonide foam as a new therapeutic

- principle in distal ulcerative colitis in comparison with mesalazine enema. An open, controlled, randomized and prospective multicenter pilot study, *Z Gastroenterol*, 38 (2000) 287-293.
- [11] W.J. Sandborn, B. Bosworth, S. Zakko, G.L. Gordon, D.R. Clemmons, P.L. Golden, R.L. Rolleri, J. Yu, A.C. Barrett, E. Bortey, C. Paterson, W.P. Forbes, Budesonide foam induces remission in patients with mild to moderate ulcerative proctitis and ulcerative proctosigmoiditis, *Gastroenterology*, 148 (2015) 740-750 e742.
- [12] G. Jena, P.P. Trivedi, B. Sandala, Oxidative stress in ulcerative colitis: an old concept but a new concern, *Free Radic Res*, 46 (2012) 1339-1345.
- [13] M.B. Grisham, Oxidants and free radicals in inflammatory bowel disease, *Lancet*, 344 (1994) 859-861.
- [14] N.J. Simmonds, D.S. Rampton, Inflammatory bowel disease--a radical view, *Gut*, 34 (1993) 865-868.
- [15] U. Dagli, M. Balk, D. Yucel, A. Ulker, H. Over, G. Saydam, B. Sahin, The role of reactive oxygen metabolites in ulcerative colitis, *Inflamm Bowel Dis*, 3 (1997) 260-264.
- [16] F. Karmeli, R. Eliakim, E. Okon, A. Samuni, D. Rachmilewitz, A stable nitroxide radical effectively decreases mucosal damage in experimental colitis, *Gut*, 37 (1995) 386-393.
- [17] S. Cuzzocrea, M.C. McDonald, E. Mazzon, L. Dugo, V. Lepore, M.T. Fonti, A. Ciccolo, M.L. Terranova, A.P. Caputi, C. Thiernemann, Tempol, a membrane-permeable radical scavenger, reduces dinitrobenzene sulfonic acid-induced colitis, *Eur J Pharmacol*, 406 (2000) 127-137.
- [18] Y. Araki, H. Sugihara, T. Hattori, The free radical scavengers edaravone and tempol suppress experimental dextran sulfate sodium-induced colitis in mice, *Int J Mol Med*, 17 (2006) 331-334.
- [19] W. Sun, P.E. Sanderson, W. Zheng, Drug combination therapy increases successful drug repositioning, *Drug Discov Today*, 21 (2016) 1189-1195.
- [20] V.T. DeVita, Jr., R.C. Young, G.P. Canellos, Combination versus single agent chemotherapy: a review of the basis for selection of drug treatment of cancer, *Cancer*, 35 (1975) 98-110.
- [21] Z.B. Weinstein, A. Bender, M. Cokol, Prediction of synergistic drug combinations, *Current Opinion in Systems Biology*, 4 (2017) 24-28.
- [22] R.X. Zhang, H.L. Wong, H.Y. Xue, J.Y. Eoh, X.Y. Wu, Nanomedicine of synergistic drug combinations for cancer therapy - Strategies and perspectives, *J Control Release*, 240 (2016) 489-503.
- [23] T.M. Allen, P.R. Cullis, Liposomal drug delivery systems: from concept to clinical applications, *Adv Drug Deliv Rev*, 65 (2013) 36-48.
- [24] H. Su, J.M. Koo, H. Cui, One-component nanomedicine, *J Control Release*, 219 (2015) 383-395.
- [25] B.L. Banik, P. Fattahi, J.L. Brown, Polymeric nanoparticles: the future of nanomedicine, *Wiley Interdiscip Rev Nanomed Nanobiotechnol*, 8 (2016) 271-299.
- [26] M. Tarhini, H. Greige-Gerges, A. Elaissari, Protein-based nanoparticles: From preparation to encapsulation of active molecules, *Int J Pharm*, 522 (2017) 172-197.
- [27] G. Batist, M. Sawyer, N. Gabrail, N. Christiansen, J.L. Marshall, D.R. Spiegel, A. Louie, A multicenter, phase II study of CPX-1 liposome injection in patients (pts) with advanced colorectal cancer (CRC), *Journal of Clinical Oncology*, 26 (2008) 4108-4108.
- [28] J.M. Reid, W. Qu, S.L. Safgren, M.M. Ames, M.D. Krailo, N.L. Seibel, J. Kuttesch, J. Holcenberg, Phase I trial and pharmacokinetics of gemcitabine in children with advanced solid tumors, *J Clin Oncol*, 22 (2004) 2445-2451.

- [29] J.E. Lancet, G.L. Uy, J.E. Cortes, L.F. Newell, T.L. Lin, E.K. Ritchie, R.K. Stuart, S.A. Strickland, D. Hogge, S.R. Solomon, R.M. Stone, D.L. Bixby, J.E. Kolitz, G.J. Schiller, M.J. Wieduwilt, D.H. Ryan, A. Hoering, M. Chiarella, A.C. Louie, B.C. Medeiros, Final results of a phase III randomized trial of CPX-351 versus 7+3 in older patients with newly diagnosed high risk (secondary) AML, *Journal of Clinical Oncology*, 34 (2016) 7000-7000.
- [30] B.S. Wong, S.L. Yoong, A. Jagusiak, T. Panczyk, H.K. Ho, W.H. Ang, G. Pastorin, Carbon nanotubes for delivery of small molecule drugs, *Adv Drug Deliv Rev*, 65 (2013) 1964-2015.
- [31] K. Radad, M. Al-Shraim, R. Moldzio, W.D. Rausch, Recent advances in benefits and hazards of engineered nanoparticles, *Environ Toxicol Pharmacol*, 34 (2012) 661-672.
- [32] K.R. Vega-Villa, J.K. Takemoto, J.A. Yanez, C.M. Remsberg, M.L. Forrest, N.M. Davies, Clinical toxicities of nanocarrier systems, *Adv Drug Deliv Rev*, 60 (2008) 929-938.
- [33] S. Eskandari, T. Guerin, I. Toth, R.J. Stephenson, Recent advances in self-assembled peptides: Implications for targeted drug delivery and vaccine engineering, *Adv Drug Deliv Rev*, 110-111 (2017) 169-187.
- [34] L. Gu, A. Faig, D. Abdelhamid, K. Uhrich, Sugar-based amphiphilic polymers for biomedical applications: from nanocarriers to therapeutics, *Acc Chem Res*, 47 (2014) 2867-2877.
- [35] P. Huang, D. Wang, Y. Su, W. Huang, Y. Zhou, D. Cui, X. Zhu, D. Yan, Combination of small molecule prodrug and nanodrug delivery: amphiphilic drug-drug conjugate for cancer therapy, *J Am Chem Soc*, 136 (2014) 11748-11756.
- [36] P. Huang, M. Hu, L. Zhou, Y. Wang, Y. Pang, G. Tong, W. Huang, Y. Su, X. Zhu, Self-delivery nanoparticles from an amphiphilic covalent drug couple of irinotecan and bendamustine for cancer combination chemotherapy, *RSC Advances*, 5 (2015) 86254-86264.
- [37] T. Zhang, P. Huang, L. Shi, Y. Su, L. Zhou, X. Zhu, D. Yan, Self-Assembled Nanoparticles of Amphiphilic Twin Drug from Floxuridine and Bendamustine for Cancer Therapy, *Mol Pharm*, 12 (2015) 2328-2336.
- [38] Y. Wang, P. Huang, M. Hu, W. Huang, X. Zhu, D. Yan, Self-Delivery Nanoparticles of Amphiphilic Methotrexate-Gemcitabine Prodrug for Synergistic Combination Chemotherapy via Effect of Deoxyribonucleotide Pools, *Bioconj Chem*, 27 (2016) 2722-2733.
- [39] C. Zhang, L. Long, Y. Xiong, C. Wang, C. Peng, Y. Yuan, Z. Liu, Y. Lin, Y. Jia, X. Zhou, X. Li, Facile Engineering of Indomethacin-Induced Paclitaxel Nanocrystal Aggregates as Carrier-Free Nanomedicine with Improved Synergetic Antitumor Activity, *ACS Appl Mater Interfaces*, 11 (2019) 9872-9883.
- [40] Y. Wang, J.D. Byrne, M.E. Napier, J.M. DeSimone, Engineering nanomedicines using stimuli-responsive biomaterials, *Adv Drug Deliv Rev*, 64 (2012) 1021-1030.
- [41] M. Smet, E. Schacht, W. Dehaen, Synthesis, characterization, and modification of hyperbranched poly(arylene oxindoles) with a degree of branching of 100%, *Angew Chem Int Ed Engl*, 41 (2002) 4547-4550.
- [42] M. Li, K. Yamato, J.S. Ferguson, B. Gong, Sequence-specific association in aqueous media by integrating hydrogen bonding and dynamic covalent interactions, *J Am Chem Soc*, 128 (2006) 12628-12629.
- [43] W. Sinananwanich, M. Ueda, Synthesis of a hyperbranched polythioketal with 100% degree of branching, *Journal of Polymer Science Part A: Polymer Chemistry*, 46 (2008) 2689-2700.

- [44] B. Sun, C. Luo, H. Yu, X. Zhang, Q. Chen, W. Yang, M. Wang, Q. Kan, H. Zhang, Y. Wang, Z. He, J. Sun, Disulfide Bond-Driven Oxidation- and Reduction-Responsive Prodrug Nanoassemblies for Cancer Therapy, *Nano Lett*, 18 (2018) 3643-3650.
- [45] Ö. Topel, B.A. Çakır, L. Budama, N. Hoda, Determination of critical micelle concentration of polybutadiene-block-poly (ethyleneoxide) diblock copolymer by fluorescence spectroscopy and dynamic light scattering, *Journal of Molecular Liquids*, 177 (2013) 40-43.
- [46] H. Kim, Y. Kim, I.H. Kim, K. Kim, Y. Choi, ROS-responsive activatable photosensitizing agent for imaging and photodynamic therapy of activated macrophages, *Theranostics*, 4 (2013) 1-11.
- [47] S. Wirtz, V. Popp, M. Kindermann, K. Gerlach, B. Weigmann, S. Fichtner-Feigl, M.F. Neurath, Chemically induced mouse models of acute and chronic intestinal inflammation, *Nat Protoc*, 12 (2017) 1295-1309.
- [48] X. Sun, S. Somada, K. Shibata, H. Muta, H. Yamada, H. Yoshihara, K. Honda, K. Nakamura, R. Takayanagi, K. Tani, E.R. Podack, Y. Yoshikai, A critical role of CD30 ligand/CD30 in controlling inflammatory bowel diseases in mice, *Gastroenterology*, 134 (2008) 447-458.
- [49] B.K. Johnson, R.K. Prud'homme, Mechanism for rapid self-assembly of block copolymer nanoparticles, *Phys Rev Lett*, 91 (2003) 118302.
- [50] Q. Zhang, F. Zhang, Y. Chen, Y. Dou, H. Tao, D. Zhang, R. Wang, X. Li, J. Zhang, Structure-Property Correlations of Reactive Oxygen Species-Responsive and Hydrogen Peroxide-Eliminating Materials with Anti-Oxidant and Anti-Inflammatory Activities, *Chemistry of Materials*, 29 (2017) 8221-8238.
- [51] H. Zhang, G. Wang, H. Yang, Drug delivery systems for differential release in combination therapy, *Expert Opin Drug Deliv*, 8 (2011) 171-190.
- [52] R.B. Johnston, Monocytes and Macrophages, *New England Journal of Medicine*, 318 (1988) 747-752.
- [53] Y.R. Na, M. Stakenborg, S.H. Seok, G. Matteoli, Macrophages in intestinal inflammation and resolution: a potential therapeutic target in IBD, *Nat Rev Gastroenterol Hepatol*, (2019).
- [54] A. Lesniak, A. Salvati, M.J. Santos-Martinez, M.W. Radomski, K.A. Dawson, C. Aberg, Nanoparticle adhesion to the cell membrane and its effect on nanoparticle uptake efficiency, *J Am Chem Soc*, 135 (2013) 1438-1444.
- [55] H.U. Simon, A. Haj-Yehia, F. Levi-Schaffer, Role of reactive oxygen species (ROS) in apoptosis induction, *Apoptosis*, 5 (2000) 415-418.
- [56] S. Sedghi, J.Z. Fields, M. Klamut, G. Urban, M. Durkin, D. Winship, D. Fretland, M. Olyaei, A. Keshavarzian, Increased production of luminol enhanced chemiluminescence by the inflamed colonic mucosa in patients with ulcerative colitis, *Gut*, 34 (1993) 1191-1197.
- [57] N.J. Simmonds, R.E. Allen, T.R. Stevens, R.N. Van Someren, D.R. Blake, D.S. Rampton, Chemiluminescence assay of mucosal reactive oxygen metabolites in inflammatory bowel disease, *Gastroenterology*, 103 (1992) 186-196.
- [58] Y.C. Peng, C.L. Hsu, C.F. Tung, W.K. Chou, L.R. Huang, D.Z. Hung, W.H. Hu, D.Y. Yang, Chemiluminescence assay of mucosal reactive oxygen species in gastric cancer, ulcer and antral mucosa, *Hepatogastroenterology*, 55 (2008) 770-773.
- [59] U. Klotz, K. Maier, C. Fischer, K. Heinkel, Therapeutic Efficacy of Sulfasalazine and Its Metabolites in Patients with Ulcerative Colitis and Crohn's Disease, *New England Journal of Medicine*,

303 (1980) 1499-1502.

[60] S. Bhattacharjee, DLS and zeta potential - What they are and what they are not?, *J Control Release*, 235 (2016) 337-351.

[61] M. Mahfouz, P. Martin, A.F. Carrion, Hepatic Complications of Inflammatory Bowel Disease, *Clin Liver Dis*, 23 (2019) 191-208.

[62] A.A. Date, G. Halpert, T. Babu, J. Ortiz, P. Kanvinde, P. Dimitrion, J. Narayan, H. Zierden, K. Betageri, O. Musmanno, H. Wiegand, X. Huang, S. Gumber, J. Hanes, L.M. Ensign, Mucus-penetrating budesonide nanosuspension enema for local treatment of inflammatory bowel disease, *Biomaterials*, 185 (2018) 97-105.

[63] L. Li, J. Guo, Y. Wang, X. Xiong, H. Tao, J. Li, Y. Jia, H. Hu, J. Zhang, A Broad-Spectrum ROS-Eliminating Material for Prevention of Inflammation and Drug-Induced Organ Toxicity, *Adv Sci (Weinh)*, 5 (2018) 1800781.

[64] R.N. Brogden, D. McTavish, Budesonide, *Drugs*, 44 (1992) 375-407.